Structure of the Na,K-ATPase Regulatory Protein FXYD1 in Micelles[†]

Peter Teriete, Carla M. Franzin, Jungyuen Choi, and Francesca M. Marassi*

Burnham Institute for Medical Research, 10901 North Torrey Pines Road, La Jolla, California 92037

Received February 26, 2007; Revised Manuscript Received April 12, 2007

ABSTRACT: FXYD1 is a major regulatory subunit of the Na,K-ATPase and the principal substrate of hormone-regulated phosphorylation by c-AMP dependent protein kinases A and C in heart and skeletal muscle sarcolemma. It is a member of an evolutionarily conserved family of membrane proteins that regulate the function of the enzyme complex in a tissue-specific and physiological-state-specific manner. Here, we present the three-dimensional structure of FXYD1 determined in micelles by NMR spectroscopy. Structure determination was made possible by measuring residual dipolar couplings in weakly oriented micelle samples of the protein. This allowed us to obtain the relative orientations of the helical segments and information about the protein dynamics. The structural analysis was further facilitated by the inclusion of distance restraints, obtained from paramagnetic spin label relaxation enhancements, and by refinement with a micelle depth restraint, derived from paramagnetic Mn line broadening effects. The structure of FXYD1 provides the foundation for understanding its intra-membrane association with the Na,K-ATPase α subunit and suggests a mechanism whereby the phosphorylation of conserved Ser residues, by protein kinases A and C, could induce a conformational change in the cytoplasmic domain of the protein to modulate its interaction with the α subunit.

The Na,K-ATPase is the principal enzyme responsible for maintaining the gradient of Na and K ion concentrations across cell membranes. The energy required to pump ions into and out of cells is generated by the hydrolysis of ATP in the cytosol through a process that involves distinct phosphorylated intermediates of the enzyme with different affinities for Na and K ions. The enzyme complex is formed by a catalytic α subunit (110 kD), formed by 10 membrane-spanning helices and 2 large cytoplasmic loops that fold into 4 distinct functional domains, an auxiliary *β* subunit (31 kD), with 1 membrane-spanning helix and a highly glycosylated extracellular domain, and a third regulatory subunit (7−17 kD) that modulates the enzyme kinetics, with 1 membrane-spanning helix and variable extra and intracellular domains. The tissue-specific homologues of this third subunit belong to the FXYD protein family, which derives its name from a highly conserved signature sequence of amino acids (Phe-X-Tyr-Asp) preceding the transmembrane domain. The FXYD proteins, first discovered associated with the Na,K-ATPase in kidney membranes and in heart sarcolemma, have been the focus of recent attention due to their ability to finely regulate the activity of the enzyme complex in various physiological settings (*1*−*4*).

The FXYD genes are expressed predominantly in tissues that are electrically excitable or that specialize in transport. Six of the seven mammalian FXYD family members and the shark homologue have been shown to interact specifically with the Na,K-ATPase and to modulate its functional properties in a tissue-specific and physiological-state-specific manner, and their effects on the enzyme's rate constant and its affinity for intracellular Na or extracellular K ions have been described (*1*−*4*). While some FXYD proteins increase the Na affinity, thereby activating the enzyme's function at lower Na concentrations, others have the opposite effect, and these contrasting activities have been ascribed, in part, to specific differences in amino acids of the FXYD transmembrane domains, which are otherwise highly homologous throughout the protein family across species. The FXYD functions are further modulated by their cytoplasmic domains, which may associate with different regions of the α subunit to regulate enzymatic activity, and by post-translational modifications including phosphorylation (FXYD1[1]) and glycosylation (FXYD5).

In heart and skeletal muscle sarcolemma, FXYD1 (PLM; phospholemman) is an integral part of the Na,K-ATPase enzyme complex (*5*, *6*), where it plays a role in regulating muscle contractility. It is also the principal substrate of hormone-stimulated phosphorylation by c-AMP-dependent protein kinases A and C (PKA and PKC) and other kinases (*6*−*8*), and its activity in different physiological settings is affected by its phosphorylation state (*9*−*12*). In addition, FXYD1 as well as at least three other FXYD family members can induce ionic currents in *Xenopus* oocytes and in

[†] This research was supported by a grant from the National Institutes of Health (CA082864). The NMR studies utilized the Burnham Institute NMR Facility, supported by a grant from the National Institutes of Health (CA030199).

* To whom correspondence should be addressed. Phone: 858-795-5282. Fax: 858-713-6268. E-mail: fmarassi@burnham.org.

[1] Abbreviations: Da, magnitude of the alignment tensor; DTT, dithiothreitol; FXYD1, phospholemman, plm; GDO, generalized degree of order; HSQC, heteronuclear single quantum correlation; MTSL, 1-oxy-2,2,5,5-tetramethyl-*d*-3-pyrroline-3-methyl; NMR, nuclear magnetic resonance; NOE, nuclear Overhauser effect; NOESY, nuclear Overhauser effect spectroscopy; PAGE, polyacrylamide electrophoresis; PKA, protein kinase A; PKC, protein kinase C; PRE, paramagnetic relaxation enhancement; R, rhombicity of the alignment tensor; RDC, residual dipolar coupling; rmsd, root mean square deviation; SDS, sodium dodecyl sulfate.

10.1021/bi700391b CCC: $37.00
Published on Web 05/19/2007

phospholipid bilayers (*13*, *14*); however, the direct formation of ion channels has not been demonstrated *in vivo*, and recent evidence indicates that the role of FXYD proteins in ion transport regulation is solely related to their association with the Na,K-ATPase and other ion transporters.

High-resolution structures of the α subunit nucleotide binding domain (*15*, *16*) and of its fifth transmembrane helix (*17*) have been determined by NMR or X-ray crystallography, and the structure of the Na,K-ATPase complex has been determined at 9.5 Å resolution by cryo-electron microscopy analysis of two-dimensional crystals of native kidney membranes (*18*). In this structure, the electron density map clearly identifies the arrangement of the 10 transmembrane helices of the α subunit as well as distinct regions assigned to the transmembrane domains of the *β* and FXYD subunits. The map indicates that the FXYD protein associates with the α subunit in a groove, which was assigned to transmembrane helices M2, M4, M6, and M9 by homology modeling based on the 2.6 Å resolution crystal structure of the Ca-ATPase (*19*). This interaction has been confirmed by cross-linking and mutational studies, showing that the FXYD transmembrane domains associate in close proximity to transmembrane helices M2 and M9 of the α subunit (*20*, *21*).

Recently, we reported that the helical structures of FXYD1, FXYD3, and FXYD4 in micelles mirror the intron−exon structures of their corresponding genes (*22*). Although the FXYD proteins are relatively small, ranging from about 60 to 160 amino acids, they are all encoded by genes with 6 to 9 small exons, which is highly suggestive of modular gene assembly. The coincidence of helical regions and connecting segments with the positions of intron−exon junctions in the genes indicates that the proteins are assembled from discrete structured domains, which may serve to confer different functional properties in various physiological settings.

Here, we present the three-dimensional (3D) structure of FXYD1 determined in micelles by NMR spectroscopy. Structure determination was made possible by the measurement of residual dipolar couplings (RDCs) in weakly oriented samples of FXYD1 in micelles to obtain the relative orientations of the helical segments of the protein. The orientation-dependent information, derived from RDCs, provides very high-resolution restraints for structure determination and refinement of both globular and membrane proteins as well as detailed information about protein dynamics (*23*−*26*), and in our previous FXYD study, the RDCs measured from backbone sites in FXYD1, FXYD3, and FXYD4 were instrumental for the identification of helix breaks that map with the genetic structures (*22*). Typically, the selection of one correct orientation among the set of four symmetric degenerate solutions consistent with the RDC data requires the measurement of RDCs in two different alignment media. In this study, however, the RDC analysis was facilitated by considering the protein structure in the frame of the lipid bilayer membrane and by implementing a micelle depth restraint during structure refinement. The inclusion of this additional membrane-protein-specific restraint may be generally useful for structure determination with RDCs. The structure of FXYD1 provides some insight for the association of FXYD1 with the Na,K-ATPase α subunit and paves the way for structure determination within the enzyme complex.

MATERIALS AND METHODS

Sample Preparation. FXYD1 was expressed, purified, and characterized as described previously (*27*). SDS-PAGE was performed with the Tris-Tricine system (*28*), and gels were stained with Coomassie Blue. Solution NMR samples were prepared by dissolving pure lyophilized FXYD1 in 300 μL of buffer (20 mM sodium citrate at pH 5, 10 mM DTT, 10% D_2O, and 500 mM SDS). To measure RDCs, the samples were weakly aligned in 7% polyacrylamide gels by means of either vertical compression or expansion, as described previously (*22*). For the spin-label-induced paramagnetic relaxation enhancement (PRE) experiments, one of the cysteines in the sequence of FXYD1 was changed to serine (C40S) using the QuickChange mutagenesis kit (Strategene). The remaining single cysteine (Cys42) was modified by reaction with the paramagnetic spin label 1-oxy-2,2,5,5-tetramethyl-*d*-3-pyrroline-3-methyl (MTSL; Toronto Research Chemicals) or its acetylated diamagnetic analogue 1-acetoxy-2,2,5,5-tetramethyl-*d*-3-pyrroline-3-methyl. Both reactions were performed in parallel, with two equal portions of purified FXYD1(C40S), as described by Tamm and co-workers (*29*). For the Mn-induced PRE experiments, the resonance intensities in the $^1H/^{15}N$ HSQC spectrum of FXYD1 were measured after the addition of $MnCl_2$ to the micelle sample, to final concentrations of 0.5, 0.8, or 1.6 mM.

NMR Experiments. The $^1H/^{13}C/^{15}N$ NMR experiments, used to assign resonances, measure chemical shifts, $^1H/^{15}N$ RDCs, hydrogen exchange profiles, and ^1H-^{15}N heteronuclear NOEs for the FXYD family proteins, were described previously (*22*). NOEs were obtained using the 3D ^{15}N-NOESY-HSQC experiment (*30*) with a NOESY mixing time of 150 ms. NOE intensities were measured and calibrated using known inter-proton distances in regions of regular secondary structure and converted into three distance restraint categories with ranges of 1.8−2.7, 1.8−3.5, and 1.8−5.0 Å. All NMR experiments were performed at 40 °C. The chemical shifts were referenced to the ^1H_2O resonance, set to its expected position of 4.5999 ppm at 40 °C (*31*). NMR experiments were performed on a Bruker AVANCE 600 MHz spectrometer. The NMR data were processed using NMRPipe (*32*), and the spectra were assigned and analyzed using Sparky (*33*).

Analysis of MTSL PRE Data. The MTSL PRE data were analyzed as described by Battiste and Wagner (*34*). The global correlation time of the protein-detergent micelle (10 ns) was taken from the values measured by Girvin and co-workers for micelle samples of membrane proteins with size and aggregation state similar to those of FXYD1 (*35*). The PRE distance restraints were divided in three categories with ranges of <15, 15−21, and >21 Å. In the working PRE range of 15−21 Å, a 50% uncertainty in the correlation time corresponds to an uncertainty of ±1 Å in the calculated distance. To account for uncertainty in the correlation time and in the conformation of the MTSL label, we used upper and lower limits of ±1.5 Å in the structure calculations.

Structure Calculations. Structure calculations were performed with the program XPLOR-NIH (*36*). Order tensor analysis of the RDC data and analysis of molecular fragment orientations were performed with the program REDCAT (*37*). *R* factors for the RDC data were calculated as described

by Clore and Garrett (*38*). Dihedral angles were derived from the analysis of chemical shifts with the program TALOS (*39*). Coordinate rotations and translations were performed using MacPyMol (DeLano Scientific LLC) or Fortran scripts. Structures were rendered in MacPymol. The protein surface electrostatic potential was calculated with the program GRASP (*40*), with inner and outer dielectric constants of 4 and 80, respectively. Structures were validated with PROCHECK (*41*). All calculations were performed on a 2.16 GHz Intel Core Duo MacBook Pro running OS X 10.4.8.

A starting structure was generated from extended random coil coordinates using a high-temperature-simulated annealing protocol (*42*) with XPLOR-NIH internal dynamics (*43*). Dihedral angle restraints were imposed by a quadratic harmonic potential with a force constant of 400 kcal mol^{-1} rad^{-2}. Hydrogen bonds for backbone sites in the transmembrane helix (residues 18−38) were derived from hydrogen exchange profiles (*22*) and imposed by restraining the O-H distances to 2 ± 0.2 Å and the O-N distances to 3 ± 0.2 Å, with a force constant of 50 kcal mol^{-1} $Å^{-2}$. Distance restraints derived from NOEs were imposed by a flat-well harmonic potential with a force constant of 50 kcal mol^{-1} $Å^{-2}$. The torsion angle database Rama potential (*44*) was used with a force constant of 0.2 to select preferred side chain conformations relative to the backbone dihedral angles. Other force constants were as described by Nilges and co-workers (*42*).

A second simulated annealing step was performed at low temperature (*45*) to impose RDC restraints with the XPLOR-NIH SANI potential (*46*). In this step, we used only the RDCs measured for residues in helical segments of the protein, with similar degree of order and with values of the heteronuclear $^1H/^{15}N$ NOE greater than 0. During simulated annealing, the temperature was cooled from 300 to 20 K in steps of 10 K, with 7 ps of internal dynamics at each temperature, the RDC restraint force constant was ramped from 0.01 to 5.0 kcal Hz^{-2}, the NOE and hydrogen bond distance restraint force constants were ramped from 2 to 20 kcal mol^{-1} $Å^{-2}$, the dihedral angle restraint force constant was held at 300 kcal mol^{-1} rad^{-2}, and the Rama potential force constant was held at 0.2. The other force constants were as described by Bax and co-workers (*45*).

A third simulated annealing step was performed with semi-rigid-body internal dynamics to link the molecular fragments in their correct relative positions. In this step, the coordinates of the backbone atoms (N, O, C, CA, HA, and HN) of residues 13−43 were fixed, while those of residues 60−69 were grouped as a rigid body that was allowed to undergo translational, but not rotational, motion. The atoms in the side chains and the termini and connecting loop were allowed both rotational and translational degrees of freedom. Spin label PREs were imposed by restraining the OS1-HN distances between the paramagnetic oxygen atom of MTSL and the backbone amide proton, with a force constant of 40 kcal mol^{-1} $Å^{-2}$. The MTSL parameter and topology files developed by Battiste and Wagner (*34*), available with the XPLOR-NIH package, were used. Dihedral angle and NOE restraints were imposed with force constants of 400 kcal mol^{-1} rad^{-2} and 40 kcal mol^{-1} $Å^{-2}$, respectively. Mn PRE restraints were implemented by applying harmonic coordinate plane restraints with a force constant of −300 kcal mol^{-1} $Å^e$ to the backbone HN atoms of residues 60 and 68 to restrict their translational motion within an *xz* plane parallel to the membrane surface.

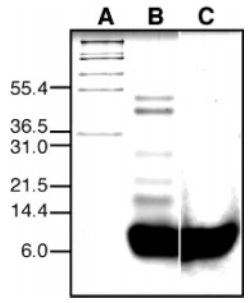

FIGURE 1: SDS-PAGE of purified FXYD1 obtained with or without the reducing agent β-mercaptoethanol. (A) Molecular weight markers. (B) FXYD1 without β-mercaptoethanol. (C) FXYD1 with β-mercaptoethanol.

RESULTS AND DISCUSSION

Oligomerization State. FXYD1 has been shown to induce ionic conductance when it is expressed in *Xenopus* oocytes or when it is incorporated in planar lipid bilayers (*13*, *14*), and similar observations have been made for its homologues FXYD2−4 (*1*−*4*), raising the possibility that channel formation could be another mechanism by which the proteins regulate ion transport across the plasma membrane. Recent studies, however, showed that FXYD3 has no effect on chloride conductance across the membranes of T3M4 pancreatic cancer cells where it is overexpressed (*47*) and that FXYD4 modulates ionic currents through its interaction with the KCNQ1 depolarization activated channels (*48*). Furthermore, ion channel formation would entail protein homo-oligomerization; however, there is no evidence of FXYD1 or other FXYD proteins associating as homo-multimeric assemblies, free from Na,K-ATPase. In contrast, phospholamban, the Ca-ATPase regulatory protein to which channel activity is also ascribed, can adopt a pentameric structure in SDS and other detergents (*49*−*51*).

On SDS-PAGE, in the presence of reducing agent, FXYD1 migrates with an estimated molecular mass corresponding to that of the monomeric protein (8.4 kD; Figure 1C), whereas in the absence of reducing agent, bands corresponding to dimers and higher order aggregates, up to hexamers (50.4 kD; Figure 1B), are also seen. We have observed similar results for the other family members, FXYD2−FXYD5, indicating that they are also monomeric in SDS and that oligomerization is through the formation of disulfide bonds between the free Cys side chains. Indeed, we have found that a mutant of FXYD3, where all four cysteines in the sequence are changed to serine, always migrates as a single band corresponding to monomer in both SDS and PFO, a detergent that has been shown to maintain the quaternary oligomeric structures of membrane proteins (*52*). In all FXYD proteins, the cysteines are exposed to the reducing environment of the cytoplasm or the plasma membrane and do not participate in disulfide bonds. Two independent electrophoresis studies found that 20-residue peptides corresponding to the transmembrane domains of FXYD1 (*53*) or FXYD2 (*54*), where no cysteines are present, migrate as monomers in SDS but form oligomers in PFO. While the results from the FXYD1 peptide were suggested to reflect channel formation, the propensity for self-associa-

tion in the FXYD2 peptide was interpreted as a reflection of its ability to associate with the transmembrane domain of the Na,K-ATPase α subunit rather than intrinsic channel activity.

In NMR studies of membrane proteins, very high detergent concentrations are typically used to ensure the presence of no more than one protomer per micelle (one protein per micelle for monomers or one protein complex per micelle for oligomers). In our NMR samples, where the critical micelle concentration is estimated to be 4 mM and the aggregation number 90 (*55*), the probability of finding more than one protein per micelle is 0.93 at 25 mM SDS but decreases to 0.08 at 200 mM SDS and plateaus to 0.02 at 400 mM SDS.

Association with the Micelle. We examined the $^1H/^{15}N$ HSQC spectra of FXYD1−FXYD4 in several well-characterized micelle-forming detergents and obtained the best results in SDS micelles (*56*). Although SDS is widely assumed to be a universal protein-denaturing detergent because of its common use in protein electrophoresis, many integral membrane proteins retain their structures in SDS micelles (*57*). Because the majority of functional and structural studies of Na,K-ATPase have been done on enzyme purified in the presence of SDS (*18*), and the noncovalent associations of α, β and FXYD subunits are maintained through the SDS purification process, we reasoned that this detergent would also be a good choice for FXYD structural studies.

Previously, we showed that the secondary structure of FXYD1 mirrors its genetic organization, with helix breaks occurring at the sites of the intron-exon junctions of the gene (*22*). The overall structural features are summarized in Figure 2B. The transmembrane helix (H2) is preceded by a short helical segment (H1) of approximately five residues, beginning at Asp12 of the FXYD signature sequence, and is followed by a third short helix (H3), spanning the conserved basic RRCRCK sequence of the protein. The $^1H/^{15}N$ heteronuclear NOEs (Figure 2C) and the HSQC peak intensities (Figure 2D; black bars) indicate that H1, H2, and H3 have similar backbone dynamics. A fourth helix (H4), containing the S63 and S68 consensus sites for phosphorylation by PKA and PKC, is separated from H3 by a flexible linker with significantly smaller values of the $^1H/^{15}N$ NOE and significantly greater peak intensities.

To probe the association of FXYD1 with the micelle, we examined the effect of $MnCl_2$ on the $^1H/^{15}N$ HSQC spectrum. The paramagnetic electrons in the Mn ion induce distance-dependent broadening of peaks from protein sites that are solvent-exposed, whereas residues in the hydrophobic interior of the micelle, such as those in transmembrane helices, are mainly unaffected. The addition of $MnCl_2$ to FXYD1 resulted in substantial line broadening and disappearance of peaks from amino acids in the N- and C-terminal regions of the protein in H1 and in the flexible linker (Figure 2D and E). In contrast, peaks from H2 and H3 retained significant or full intensity, indicative of association with the micelle. Notably, the peaks from residues in H4 also retained much of their intensity, indicating that this region of the protein also associates strongly with the hydrophobic micelle.

The Mn PRE profile in Figure 2E displays the residual intensity measured for each peak after the addition of $MnCl_2$ and reflects the depth of insertion of the respective protein

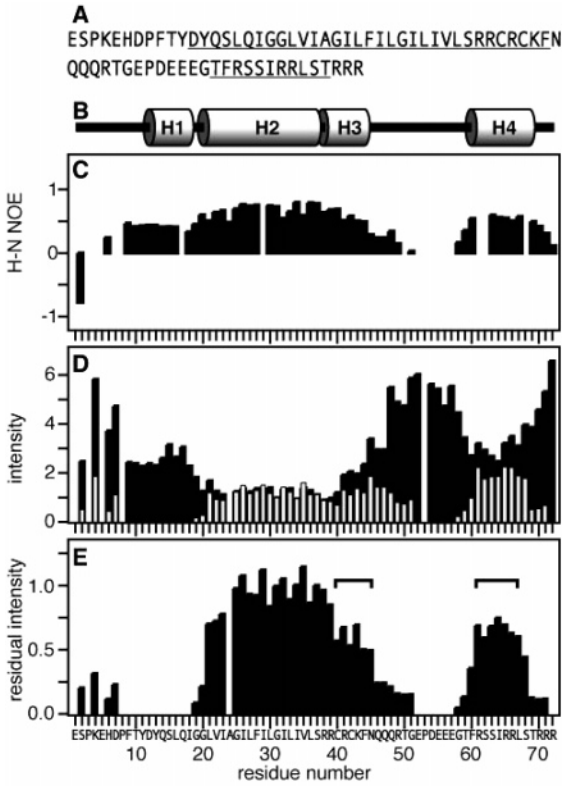

FIGURE 2: Effect of Mn-induced PRE on the resonance intensities. (A) Amino acid sequence of human FXYD1 with helical regions underlined. Residue numbering begins at 1 after the signal sequence (NCBI protein accession: NP_068702). (B) Protein secondary structure. (C) $^1H/^{15}N$ heteronuclear NOEs. (D) Normalized $^1H/^{15}N$ HSQC peak intensities obtained without (I_{-Mn}, black bars) or with (I_{+Mn}, gray bars) 1.6 mM $MnCl_2$. Positions that are left blank correspond to prolines (P3, P8, and P53) or overlapped resonances (E5 and A24). (E) Residual normalized peak intensity (I_{-Mn}/I_{+Mn}). The horizontal square brackets mark residues in H3 and H4 with similar protection from aqueous Mn.

sites in the micelle. The profile indicates that residues 60−68 in H4 are protected from interaction with the aqueous Mn ions to a similar extent as for residues 39−45 in H3, indicating that both segments are buried at a similar depth within the micelle. Residues 22−38, in the transmembrane helix (H2), are buried deeper in the micelle because their amide HN resonances retain nearly 100% of their intensity after the addition of $MnCl_2$. In contrast, peaks from H1 and sites in the flexible loop and in the termini experience a total or substantial loss of resonance intensity in the presence of Mn, reflecting the exposure of these sites to the aqueous environment. Because the Mn PRE profile effectively serves as a ruler for the depth of insertion of FXYD1 in the micelle, we implemented it as a restraint to define the relative positions of the helices in the structure calculations.

Structure Determination. Structure determination relied primarily on restraints from RDCs, dihedral angles, H/D exchange measurements, Mn PREs, and MTSL PREs. No long-range NOEs could be identified connecting helix H4 to the rest of the protein across the 10-residue flexible linker. In a first stage of simulated annealing, a starting structure was generated using dihedral angles, hydrogen bonds, and short- or medium-range NOEs but no RDCs. Order tensor analysis of the RDC data yielded similar values of the alignment tensor's magnitude (Da = 12.7), rhombicity

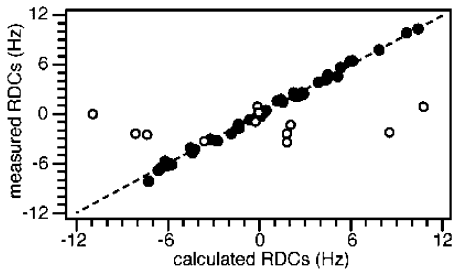

FIGURE 3: Correlation between HN RDCs measured experimentally and HN RDCs back-calculated from the refined structure of FXYD1. The RDCs from the flexible linker and termini (○) correlate poorly with those from the helical region of the protein (●; rmsd = 0.31; *R* factor = 0.07).

(R = 0.4), and generalized degree of order (GDO = 0.00074) for residues in the helical regions of the protein, indicating that they experience similar ordering in the aligned detergent micelles. Because H4 is connected to the rest of the protein by a long flexible segment, the observation of a common order tensor reflects the independent association of the transmembrane and cytoplasmic helical regions with the micelle. In contrast, the flexible loop and termini have a substantially reduced and completely different degree of order. A second stage of simulated annealing, performed at low temperature with the RDC restraints, yielded a refined structure with excellent agreement (rmsd = 0.31; *R* factor = 0.07) between experimental and calculated RDCs across all four helical regions of the protein (Figure 3).

The relative orientations of helices H1−H3 are well defined by the dihedral angles and the RDCs. However, because H4 is loosely connected to the rest of the protein, this initial refined structure represents only one of four possible orientations of H4 that are consistent with the RDC data. To determine the orientation of helix H4, two molecular fragments were generated by dividing the coordinates of the refined initial structure into two sets for independent order tensor analysis with the experimental RDCs.

Fragment A (residues 1−50) includes helices H1−H3, and fragment B (residues 51−72) includes the flexible linker and helix H4. Rotation of each molecular fragment into the principal axis frame of its order tensor, followed by 180° rotations around the principal Sxx, Syy, or Szz axes to generate four degenerate orientations, yielded four possible combinations of fragment A with fragment B, each consistent with the experimental RDCs (Figure 4). The selection of a single fragment combination among these four degenerate solutions was made possible by further rotating the fragments in the frame of the membrane and considering the Mn PRE profile as well as the amphiphilic character of H4, which dictates the sidedness of its association with the membrane-water or micelle-water interface.

The absolute orientation of fragment A in the membrane is not determined by the solution NMR data obtained in micelles; however, we found that by viewing the structure in the membrane frame, there is only one solution for fragment B (Figure 4, solution I) that can simultaneously satisfy both the Mn PRE data and the amphiphilic polarity of amino acids in helix H4, with apolar residues (Phe60, Ile64, and Leu67) facing the membrane interior and charged residues (Arg61, Arg65, and Arg66) facing the aqueous exterior. The Arg hydrocarbon side chains are sufficiently long to reach the membrane surface, while allowing H4 to penetrate the membrane below the water−lipid interface. Solution I is also consistent with the solid-state NMR spectra of FXYD1 in lipid bilayers, which indicate the presence of a helical segment associated with the membrane surface (*56*). Solution II, however, has an opposite amphiphilic polarity to the membrane, with apolar side chains facing out and charged side chains facing in.

The membrane Y and Z axes were selected to allow the transmembrane helix to cross the membrane at an angle of 15°, in agreement with the solid-state NMR data for FXYD1 and other FXYD proteins in oriented lipids bilayers (*56*). Rotation around the membrane X axis satisfies both the 15° transmembrane tilt and the amino acid amphiphilic polarity

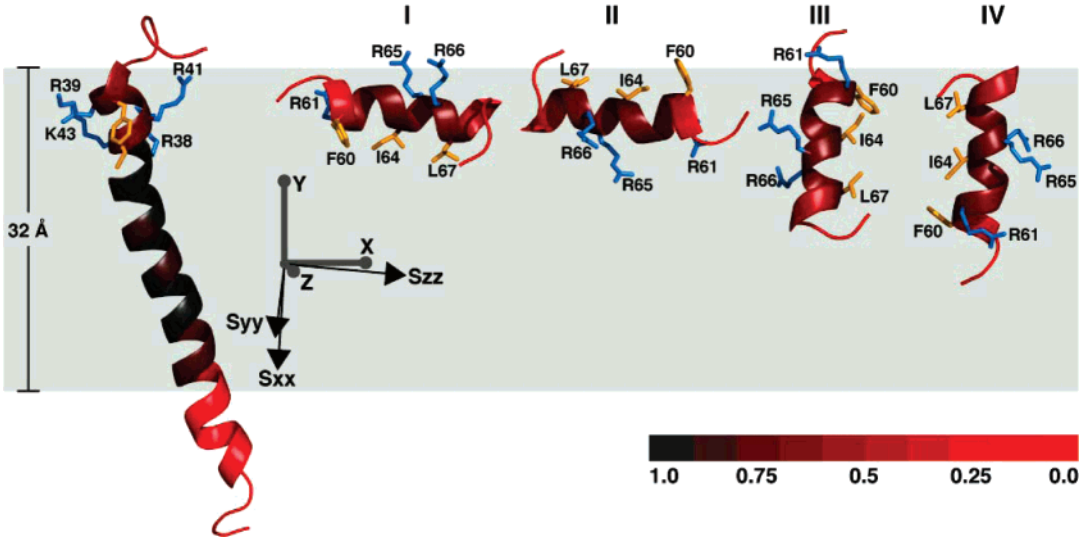

FIGURE 4: Molecular fragments of FXYD1 oriented in the frame of the alignment tensor (Sxx, Syy, and Szz; black axes) and of the membrane (X, Y, Z; gray axes). Fragment A (shown at left) can be linked with one of four possible orientations of fragment B (I−IV). The red color gradation reflects the degree of protection from Mn-induced PRE, with full protection in the center of the membrane (gray) and no protection outside the membrane (red). The total Mn protection profile corresponds to a length of 32 Å along the membrane Y axis. Side chains from basic residues in helix H3 (R37, R39, R41, and K43) and helix H4 (R61, R65, and R66) are shown in blue. Side chains from apolar residues in H3 (C40, C42, and F44) and H4 (F60, I64, and L67) are shown in yellow.

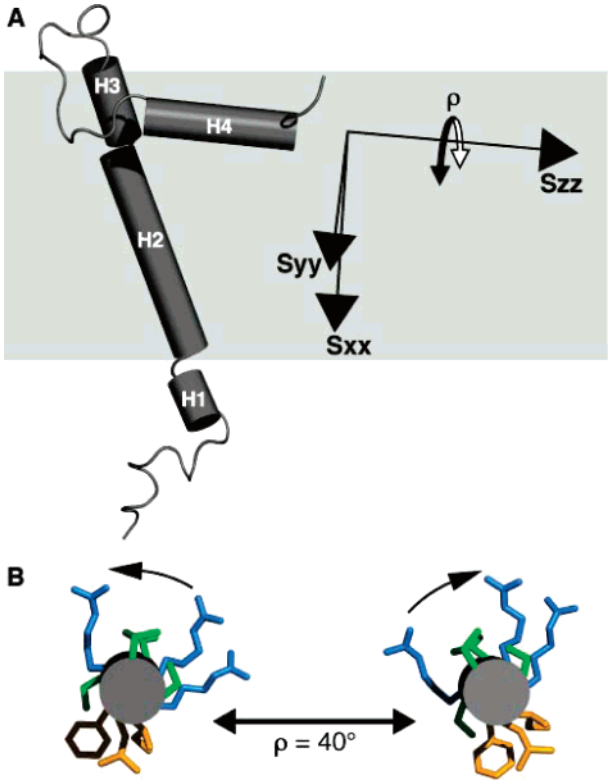

FIGURE 5: Tube representation of the FXYD1 structure in the frame of the membrane (gray box) and of the alignment tensor (Sxx, Syy, Szz). (A) Helix H4 is nearly parallel to Szz. This is consistent with helix reorientation around Szz, resulting both in a GDO value similar to that of helices H1−H3 and greater dynamics observed from the heteronuclear NOEs and resonance intensities. (B) Helix H4 viewed from the C-terminus. A maximum helix reorientation of $\rho \approx 40°$, around Szz, maintains the amphiphilic polarity of hydrophobic and hydrophilic side chains at the membrane surface.

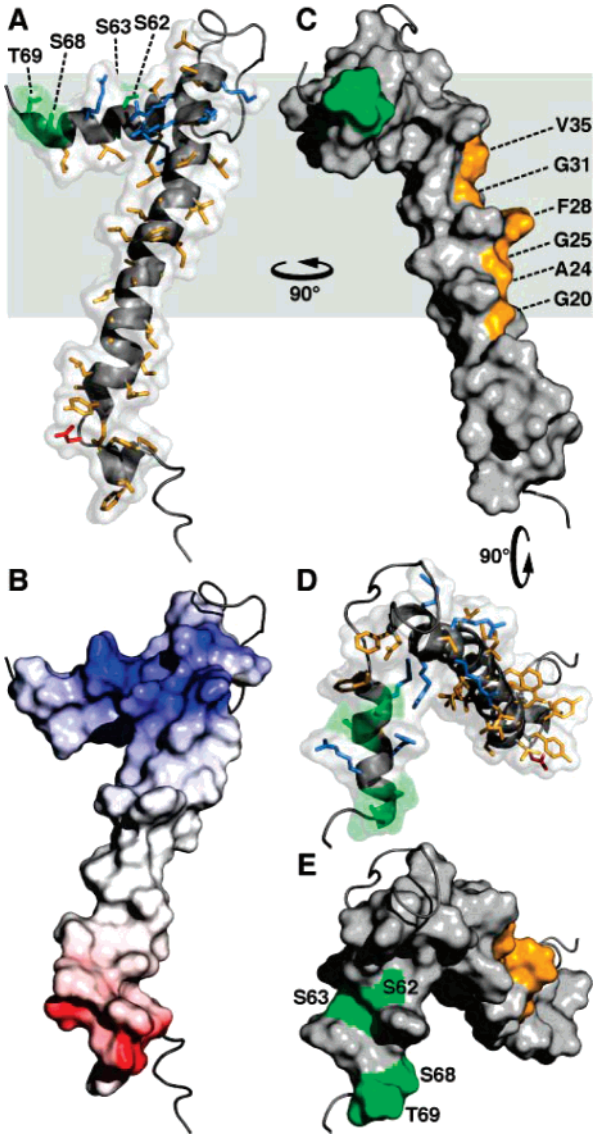

FIGURE 6: Molecular backbone and surface representations of FXYD1. (A and D) In the helical regions, basic side chains are shown in blue, acidic side chains are red, and apolar side chains are yellow. The three Ser residues (S62, S63, and S68) and Thr69 in the cytoplasmic helix are in green. (B) The surface is color coded with regions of electrostatic potential $< -8k_BT$ in red and regions of electrostatic potential $> +8k_BT$ in blue, where k_B is the Boltzmann constant, and T is the temperature. (C) The structure is viewed 90° around the membrane Y axis from A and B. Residues in the transmembrane helix (G20, A24, G25, F28, G31, and V35), predicted to interact with the Na,K-ATPase α subunit, are shown in yellow. (D and E) The structures are viewed down the membrane surface from the cytoplasm, 90° around the membrane X axis from C. The structure has been deposited in the Protein Data Bank (pdb accession code: 2JO1).

of H4. The resulting orientation of fragment A also satisfies the amphiphilic character of H3, allowing the charged Arg and Lys side chains (Arg38, Arg39, Arg41, and Lys43) to point away from the membrane interior and into the aqueous phase, which, *in vivo*, corresponds to the cytoplasm.

In the membrane frame of reference, it becomes apparent that solutions III and IV of fragment B both send H4 plunging into the hydrophobic interior of the membrane, in violation of the Mn PRE data. For example, to satisfy the Mn PRE profile of Arg61, whose amide peak retains 60−70% of its intensity in the presence of Mn, solution III would have to place Thr69, which is nearly fully exposed to Mn, at the center of the membrane hydrophobic core, at a depth similar to that of residues in the transmembrane helix that are fully protected. A similar but opposite situation is encountered with solution IV, which would have to place Thr59 (∼90% exposed) in the hydrophobic interior of the micelle to satisfy the Mn PRE profile of Leu67 (∼70% protected).

The molecular fragments were linked in their correct relative orientations and positions by a third and final simulated annealing calculation, where the backbone coordinates of residues 13−44 (H1 to H3) were fixed, while those of residues 60−69 (H4) were allowed to undergo only translational motions as a rigid group, and atoms in the termini, flexible loop, and side chains were free to undergo both rotational and translational motions. In this step, the dynamics were restrained by the PRE-derived distances between the MTSL label at Cys42 and residues in H2 and H4, by dihedral angle restraints and by short- to medium-range NOE distance restraints.

In addition, the Mn PRE micelle depths were implemented as harmonic coordinate plane restraints for the backbone HN atoms of residues 60 and 68 to confine residues in H4 within the XZ plane, parallel to the membrane surface, same as that of residue 42, which experiences a similar Mn PRE effect. The Mn PRE profile effectively places residues in H4 at a

depth similar to that of residues 39−45 in H3. The resulting structure of FXYD1 in micelles is represented in Figures 5 and 6.

Implications for Protein Dynamics. RDCs contain information about molecular orientation and dynamics and are sensitive to motions spanning a wide range of time scales. For FXYD1, although the RDC data indicate that helix H4 experiences a degree of order in the micelle similar to that of the transmembrane helix, the heteronuclear NOEs and resonance intensities indicate increased dynamics in this region. The presence of different degrees of internal motions between two domains in a protein can affect the parameters describing the degree of order and mean orientation of each domain relative to the magnetic field, and Tolman and coworkers have discussed these effects in detail (*26*).

The effects of dynamics on the generalized degree of order depend on the direction of the axis for internal dynamic reorientation relative to the alignment frame; coincidence of the reorientation axis with the Szz principal axis of the alignment tensor has the minimum effect on degree of order, whereas coincidence with the Sxx alignment axis produces the maximum effect. As seen in Figures 4 and 5, the long axis of helix H4 is nearly parallel to the Szz axis of the FXYD1 alignment tensor; therefore, a reorientation of H4 around its length, on the membrane surface, would be consistent with both a minimum effect on the degree of order and with the observation of greater dynamics in this region of the protein. Although the extent of helix H4 reorientation cannot be gauged by the data, inspection of the structure suggests that rotational excursions as large as 40° ($\rho = 40°$; Figure 5B) would be consistent with maintaining the helix amphiphilic polarity with respect to the micelle surface, with apolar residues facing the membrane interior and polar residues facing out.

Structure of FXYD1. Different representations of the resulting structure for FXYD1 in micelles are shown in Figure 6. The structure coordinates have been deposited in the Protein Data Bank (pdb accession code: 2JOL). The FXYD motif forms a disordered segment, albeit with some propensity for helical structure, preceding the short helix H1 (Figure 6A). The function of the FXYD sequence is still unclear, although one study has shown that it is required for the stable interaction of FXYD2 or FXYD4 with the α subunit (*58*). Alternatively, the FXYD sequence could constitute a sorting or localization signal.

In the transmembrane helix of FXYD1, the Phe28 aromatic ring forms a significant protrusion out of a groove lined by small residues (Gly20, Ala24, Gly25, Gly31, and Val35) along one side of the length of the helix (Figure 6C). The Gly residues at positions 20 and 31 are fully conserved in the sequences of all FXYD proteins across species (Figure 7), and positions 24, 25, and 35 typically take small side chains (Ala, Gly, Val, or Leu). Position 28, however, displays more variability in the type and size of amino acid that it can accommodate and is occupied by Phe in FXYD1, FXYD2, and FXYD5−7, or by the smaller residues Cys and Ala in FXYD3 and FXYD4 (human sequences). A recent study showed that a Cys residue placed at position 28 (FXYD1 numbering) in the transmembrane helices of FXYD1, FXYD2, and FXYD4 allows cross-linking to the α subunit M2 transmembrane helix (*20*), as first suggested by the cryo-electron microscopy structure (*18*).

FIGURE 7: Amino acid sequences of the transmembrane domains from the human FXYD proteins. The fully conserved Gly residues, at positions 20 and 31 are highlighted in gray and marked by black circles. Other key residues, at positions 24, 25, 28 and 35, are marked by white circles. Residue numbering is according to FXYD1.

Table 1: NMR and Structure Refinement Statistics

Experimental Restraints Used in Structure Calculation and Refinement	
NOE distance restraints	447
hydrogen bond distance restraints	17
MTSL PRE distance restraints	18
HN RDC orientation restraints	55
dihedral angle restraints	41
Mn PRE harmonic restraints	2
Structure Statistics (rmsd)[a]	
violations from restraints	
distance restraints rsmd (Å)	0.082
dihedral angle restraints rsmd (°)	2.029
HN RDC restraints rsmd (Hz)	0.310
HN RDC R factor[b] (Hz)	0.070
deviation from idealized geometry	
bonds (Å)	0.005
angles (°)	0.804
impropers (°)	0.764
ϕ/Ψ in the most favored region[c] (%)	88.5
average pairwise rmsd[d]	
backbone atoms (Å)	0.128
heavy atoms (Å)	7.515
average rmsd from mean structure[d]	
backbone atoms (Å)	0.882
heavy atoms (Å)	5.257

[a] Calculated for 20 lowest energy structures out of a total 40 calculated structures. [b] Calculated according to Clore and Garrett (*38*). [c] Calculated with PROCHECK. [d] Calculated for the structured regions of the protein from residues 13−44 and 60−69.

The very high conservation of amino acids in the transmembrane helices of all FXYD proteins suggests their involvement in specific intramembrane helix-helix interactions with Na,K-ATPase and possibly other partners, and it is tempting to speculate that the specific activities of the FXYD proteins are related, in part, to subtle differences in their transmembrane sequences. For example, while FXYD2 (Phe at position 28) reduces the Na affinity of the Na,K-ATPase, FXYD4 (Ala at position 28) increases it, and their opposing activities and unique expression patterns in distinct segments of the kidney help define the physiological differences in Na,K-ATPase activity among the kidney nephron segments (*1*−*4*). Furthermore, in kidney membranes, the transmembrane helix of FXYD2 associates with the transmembrane domain of the α subunit, whereas the mutation G41R (corresponding to position 31 in FXYD1) causes misrouting of the protein by inhibiting its association with Na,K-ATPase and is linked with renal or intestinal familial hypomagnesemia (*59*). The data, therefore, indicate that the conserved Gly residue at this position plays a role

in mediating helix-helix interactions between the FXYD transmembrane helix and Na,K-ATPase. The structure of FXYD1 shows that Gly31 and the other conserved transmembrane residues line one strip along helix H2 that is unencumbered by the cytoplasmic helix H4 and that is free to interact with the α subunit.

Helix H4 associates with the micelle surface and is buried in the micelle to a similar extent as for residues 39−45 at the end of the transmembrane segment. The Arg and Lys side chains from residues 38, 39, 41, and 43 in H3 and residues 61, 65, and 66 in H4 are sufficiently long to reach the membrane surface with their positively charged groups, thus anchoring these segments to the cytoplasmic lipid-water interface. Phosphorylation of FXYD1 by PKA and PKC has been shown to affect both its Na,K-ATPase regulatory activity and possibly its mode of association with the α subunit (*9*−*12*). In the structure, the cytoplasmic Ser residues that are phosphorylated by PKA (S68) or PKC (S63, S68) point to opposite directions of H4 (Figure 6D and E) and are exposed to the surface and available for interaction with the kinases. The other two potential phosphorylation sites, S62 and T69, are also surface-exposed.

The role of FXYD1 may be analogous to that of phospholamban, which regulates the sarcoplasmic reticulum Ca-ATPase. However, unlike FXYD1, phospholamban can exist either as a monomer or as a homo-pentamer, which may represent a channel-active form of the protein. Monomeric phospholamban forms an L-shaped helical structure, where a short N-terminal intracellular helix associates with the membrane surface, and is linked to the transmembrane helix by a short segment that contains the Ser phosphorylation site (*60*). Phosphorylation increases the dynamics of the linker (*61*) and could predispose the protein for a conformational rearrangement of the helices. However, in the pentameric form, the N-terminal helix is not membrane associated but extends out from the membrane to form a funnel-like channel structure (*49*). The observation of two types of helix orientations in phospholamban indicates a propensity for conformational rearrangement.

The cytoplasmic helix of FXYD1 is highly basic, which helps explain its propensity to associate with the negatively charged micelle surface or the cellular plasma membrane. However, it is connected to the rest of the protein by a relatively long flexible linker and therefore would be capable of undergoing reorientation to interact with the cytoplasmic domain of the α subunit. Helix reorientation from the membrane surface could be triggered by phosphorylation, which introduces repulsive negative charges at S63 and S68 in H4. Indeed, a recent study, measuring fluorescence energy transfer between fluorescent-protein-linked FXYD1 and the α subunit, suggests that phosphorylation of FXYD1 by either PKA or PKC may cause a conformational change in their intermolecular association (*12*).

Interestingly, the binding of both PKC and its substrate polypeptides to acidic phospholipids is important for phosphorylation (*62*), and it has been suggested that this lipid-binding event may serve not only to co-localize the enzyme and the substrate but also to stabilize a specific substrate conformation that can be recognized by PKC (*63*). Thus, the membrane surface association of H4 could be important for FXYD1 substrate recognition by PKC, while the addition of negatively charged phosphate groups could trigger helix reorientation, thereby providing a mechanism for modulating the interaction of FXYD1 with the α subunit.

CONCLUSIONS

The structure of FXYD1 is the first to be determined for the FXYD family of Na,K-ATPase regulatory subunits and highlights some key features that suggest its mode of association with the α subunit of the enzyme. A long groove formed by highly conserved amino acids runs parallel to the length of the transmembrane helix, delineating the likely binding interface of FXYD1 with the α subunit. The groove is interrupted by the aromatic ring of Phe28, which protrudes from the transmembrane helix near the middle of the hydrophobic lipid core. Cross-linking experiments indicate that Phe28 of FXYD1 is located near Cys145 in the M2 transmembrane helix of the α subunit (*20*). Interestingly, the proximity of Phe28 to this site also places it near Phe146 in M2, raising the possibility that aromatic ring stacking could stabilize the FXYD-α interaction within the membrane. Preliminary docking studies with the structure of FXYD1 and a model of the Na,K-ATPase generated by homology with the crystal structure of Ca-ATPase (*18*, *64*) indicate that this is possible.

FXYD1 differs from FXYD2, FXYD3, and FXYD4 in the presence of a well-defined cytoplasmic helix loosely connected to the rest of the protein by a long flexible linker. The emerging structures of FXYD2 and FXYD3 show considerably less structural order in this region, while the cytoplasmic helix of FXYD4 is more rigidly connected to the transmembrane domain. This may reflect the ability of FXYD1 to undergo helix reorientation as a means to modulate its interaction with the α subunit. Initial NMR experiments with FXYD1 phosphorylated at Ser68 by PKA indicate that phosphorylation increases the dynamics around helix H4, and it will be interesting to see whether this is accompanied by a conformational change and detachment from the lipid surface.

ACKNOWLEDGMENT

We thank Homayoun Valafar for his assistance with REDCAT and Charles Schwieters for his assistance with XPLOR-NIH. We also thank Jinghua Yu for her assistance with NMR experiments, and Denise Li and Khang Thai for their assistance with sample preparation.

NOTE ADDED AFTER ASAP PUBLICATION

This paper published ASAP on May 19, 2007 with an error in the accession code in the caption of Figure 6. The correct version of this paper published on May 29, 2007.

REFERENCES

1. Sweadner, K. J., and Rael, E. (2000) The FXYD gene family of small ion transport regulators or channels: cDNA sequence, protein signature sequence, and expression, *Genomics 68*, 41−56.
2. Crambert, G., and Geering, K. (2003) FXYD proteins: new tissue-specific regulators of the ubiquitous Na,K-ATPase, *Sci. STKE 2003*, RE1.
3. Cornelius, F., and Mahmmoud, Y. A. (2003) Functional modulation of the sodium pump: the regulatory proteins "Fixit", *News Physiol. Sci. 18*, 119−124.
4. Garty, H., and Karlish, S. J. (2006) Role of fxyd proteins in ion transport, *Annu. Rev. Physiol. 68*, 431−459.

5. Crambert, G., Fuzesi, M., Garty, H., Karlish, S., and Geering, K. (2002) Phospholemman (FXYD1) associates with Na,K-ATPase and regulates its transport properties, *Proc. Natl. Acad. Sci. U.S.A. 99*, 11476−11481.
6. Palmer, C. J., Scott, B. T., and Jones, L. R. (1991) Purification and complete sequence determination of the major plasma membrane substrate for cAMP-dependent protein kinase and protein kinase C in myocardium, *J. Biol. Chem. 266*, 11126−11130.
7. Mounsey, J. P., John, J. E., 3rd, Helmke, S. M., Bush, E. W., Gilbert, J., Roses, A. D., Perryman, M. B., Jones, L. R., and Moorman, J. R. (2000) Phospholemman is a substrate for myotonic dystrophy protein kinase, *J. Biol. Chem. 275*, 23362−23367.
8. Walaas, S. I., Czernik, A. J., Olstad, O. K., Sletten, K., and Walaas, O. (1994) Protein kinase C and cyclic AMP-dependent protein kinase phosphorylate phospholemman, an insulin and adrenaline-regulated membrane phosphoprotein, at specific sites in the carboxy terminal domain, *Biochem. J. 304*, 635−640.
9. Silverman, B. Z., Fuller, W., Eaton, P., Deng, J., Moorman, J. R., Cheung, J. Y., James, A. F., and Shattock, M. J. (2005) Serine 68 phosphorylation of phospholemman: acute isoform-specific activation of cardiac Na/K ATPase, *Cardiovasc. Res. 65*, 93−103.
10. Fuller, W., Eaton, P., Bell, J. R., and Shattock, M. J. (2004) Ischemia-induced phosphorylation of phospholemman directly activates rat cardiac Na/K-ATPase, *FASEB J. 18*, 197−199.
11. Despa, S., Bossuyt, J., Han, F., Ginsburg, K. S., Jia, L. G., Kutchai, H., Tucker, A. L., and Bers, D. M. (2005) Phospholemman-phosphorylation mediates the beta-adrenergic effects on Na/K pump function in cardiac myocytes, *Circ. Res. 97*, 252−259.
12. Bossuyt, J., Despa, S., Martin, J. L., and Bers, D. M. (2006) Phospholemman phosphorylation alters its fluorescence resonance energy transfer with the Na/K-ATPase pump, *J. Biol. Chem. 281*, 32765−32773.
13. Moorman, J. R., Ackerman, S. J., Kowdley, G. C., Griffin, M. P., Mounsey, J. P., Chen, Z., Cala, S. E., O'Brian, J. J., Szabo, G., and Jones, L. R. (1995) Unitary anion currents through phospholemman channel molecules, *Nature 377*, 737−740.
14. Moorman, J. R., Palmer, C. J., John, J. E., 3rd, Durieux, M. E., and Jones, L. R. (1992) Phospholemman expression induces a hyperpolarization-activated chloride current in Xenopus oocytes, *J. Biol. Chem. 267*, 14551−14554.
15. Hakansson, K. O. (2003) The crystallographic structure of Na,K-ATPase N-domain at 2.6A resolution, *J. Mol. Biol. 332*, 1175−1182.
16. Hilge, M., Siegal, G., Vuister, G. W., Guntert, P., Gloor, S. M., and Abrahams, J. P. (2003) ATP-induced conformational changes of the nucleotide-binding domain of Na,K-ATPase, *Nat. Struct. Biol. 10*, 468−474.
17. Underhaug, J., Jakobsen, L. O., Esmann, M., Malmendal, A., and Nielsen, N. C. (2006) NMR studies of the fifth transmembrane segment of Na+,K+-ATPase reveals a non-helical ion-binding region, *FEBS Lett. 580*, 4777−4783.
18. Hebert, H., Purhonen, P., Vorum, H., Thomsen, K., and Maunsbach, A. B. (2001) Three-dimensional structure of renal Na,K-ATPase from cryo-electron microscopy of two-dimensional crystals, *J. Mol. Biol. 314*, 479−494.
19. Toyoshima, C., Nakasako, M., Nomura, H., and Ogawa, H. (2000) Crystal structure of the calcium pump of sarcoplasmic reticulum at 2.6 A resolution, *Nature 405*, 647−655.
20. Lindzen, M., Gottschalk, K. E., Fuzesi, M., Garty, H., and Karlish, S. J. (2006) Structural interactions between FXYD proteins and Na+,K+-ATPase: alpha/beta/FXYD subunit stoichiometry and cross-linking, *J. Biol. Chem. 281*, 5947−5955.
21. Li, C., Grosdidier, A., Crambert, G., Horisberger, J. D., Michielin, O., and Geering, K. (2004) Structural and functional interaction sites between Na,K-ATPase and FXYD proteins, *J. Biol. Chem. 279*, 38895−38902.
22. Franzin, C. M., Yu, J., Thai, K., Choi, J., and Marassi, F. M. (2005) Correlation of gene and protein structures in the FXYD family proteins, *J. Mol. Biol. 354*, 743−750.
23. Bax, A., Kontaxis, G., and Tjandra, N. (2001) Dipolar couplings in macromolecular structure determination, *Methods Enzymol. 339*, 127−174.
24. Prestegard, J. H., Bougault, C. M., and Kishore, A. I. (2004) Residual dipolar couplings in structure determination of biomolecules, *Chem. Rev. 104*, 3519−3540.
25. Hus, J. C., Marion, D., and Blackledge, M. J. (2000) De novo determination of protein structure by NMR using orientational and long-range order restraints, *J. Mol. Biol. 298*, 927−936.
26. Tolman, J. R., Al-Hashimi, H. M., Kay, L. E., and Prestegard, J. H. (2001) Structural and dynamic analysis of residual dipolar coupling data for proteins, *J. Am. Chem. Soc. 123*, 1416−1424.
27. Thai, K., Choi, J., Franzin, C. M., and Marassi, F. M. (2005) Bcl-XL as a fusion protein for the high-level expression of membrane-associated proteins, *Protein Sci. 14*, 948−955.
28. Schagger, H., and von Jagow, G. (1987) Tricine-sodium dodecyl sulfate-polyacrylamide gel electrophoresis for the separation of proteins in the range from 1 to 100 kDa, *Anal. Biochem. 166*, 368−379.
29. Liang, B., Bushweller, J. H., and Tamm, L. K. (2006) Site-directed parallel spin-labeling and paramagnetic relaxation enhancement in structure determination of membrane proteins by solution NMR spectroscopy, *J. Am. Chem. Soc. 128*, 4389−4397.
30. Bax, A., and Grzesiek, S. (1993) Methodological advances in protein NMR, *Acc. Chem. Res. 26*, 131−138.
31. Cavanagh, J. (1996) *Protein NMR Spectroscopy: Principles and Practice*, Academic Press, San Diego, CA.
32. Delaglio, F., Grzesiek, S., Vuister, G. W., Zhu, G., Pfeifer, J., and Bax, A. (1995) NMRPipe: a multidimensional spectral processing system based on UNIX pipes, *J. Biomol. NMR 6*, 277−293.
33. Goddard, T. D., and Kneller, D. G. (2004) *SPARKY 3*, University of California, San Francisco, CA.
34. Battiste, J. L., and Wagner, G. (2000) Utilization of site-directed spin labeling and high-resolution heteronuclear nuclear magnetic resonance for global fold determination of large proteins with limited nuclear overhauser effect data, *Biochemistry 39*, 5355−5365.
35. Krueger-Koplin, R. D., Sorgen, P. L., Krueger-Koplin, S. T., Rivera-Torres, I. O., Cahill, S. M., Hicks, D. B., Grinius, L., Krulwich, T. A., and Girvin, M. E. (2004) An evaluation of detergents for NMR structural studies of membrane proteins, *J. Biomol. NMR 28*, 43−57.
36. Schwieters, C. D., Kuszewski, J. J., Tjandra, N., and Marius Clore, G. (2003) The Xplor-NIH NMR molecular structure determination package, *J. Magn. Reson. 160*, 65−73.
37. Valafar, H., and Prestegard, J. H. (2004) REDCAT: a residual dipolar coupling analysis tool, *J. Magn. Reson. 167*, 228−241.
38. Clore, G. M., and Garrett, D. S. (1999) R-factor, free R, and complete cross-validation for dipolar coupling refinement of NMR structures, *J. Am. Chem. Soc. 121*, 9008−9012.
39. Cornilescu, G., Delaglio, F., and Bax, A. (1999) Protein backbone angle restraints from searching a database for chemical shift and sequence homology, *J. Biomol. NMR 13*, 289−302.
40. Nicholls, A., Sharp, K. A., and Honig, B. (1991) Protein folding and association: insights from the interfacial and thermodynamic properties of hydrocarbons, *Proteins 11*, 281−296.
41. Laskowski, R. A., MacArthur, M. W., Moss, D. S., and Thornton, J. M. (1993) PROCHECK: a program to check the stereochemical quality of protein structures, *J. Appl. Crystallogr. 26*, 283.
42. Nilges, M., Clore, G. M., and Gronenborn, A. M. (1988) Determination of three-dimensional structures of proteins from interproton distance data by dynamical simulated annealing from a random array of atoms. Circumventing problems associated with folding, *FEBS Lett. 239*, 129−136.
43. Schwieters, C. D., and Clore, G. M. (2001) Internal coordinates for molecular dynamics and minimization in structure determination and refinement, *J. Magn. Reson. 152*, 288−302.
44. Kuszewski, J., Gronenborn, A. M., and Clore, G. M. (1997) Improvements and extensions in the conformational database potential for the refinement of NMR and X-ray structures of proteins and nucleic acids, *J. Magn. Reson. 125*, 171−177.
45. Chou, J. J., Li, S., and Bax, A. (2000) Study of conformational rearrangement and refinement of structural homology models by the use of heteronuclear dipolar couplings, *J. Biomol. NMR 18*, 217−227.
46. Clore, G. M., Gronenborn, A. M., and Tjandra, N. (1998) Direct structure refinement against residual dipolar couplings in the presence of rhombicity of unknown magnitude, *J. Magn. Reson. 131*, 159−162.
47. Kayed, H., Kleeff, J., Kolb, A., Ketterer, K., Keleg, S., Felix, K., Giese, T., Penzel, R., Zentgraf, H., Buchler, M. W., Korc, M., and Friess, H. (2005) FXYD3 is overexpressed in pancreatic ductal adenocarcinoma and influences pancreatic cancer cell growth, *Int. J. Cancer 118*, 43−54.

48. Jespersen, T., Grunnet, M., Rasmussen, H. B., Jorgensen, N. B., Jensen, H. S., Angelo, K., Olesen, S. P., and Klaerke, D. A. (2006) The corticosteroid hormone induced factor: a new modulator of KCNQ1 channels? *Biochem. Biophys. Res. Commun. 341*, 979−988.
49. Oxenoid, K., and Chou, J. J. (2005) The structure of phospholamban pentamer reveals a channel-like architecture in membranes, *Proc. Natl. Acad. Sci. U.S.A. 102*, 10870−10875.
50. Karim, C. B., Paterlini, M. G., Reddy, L. G., Hunter, G. W., Barany, G., and Thomas, D. D. (2001) Role of cysteine residues in structural stability and function of a transmembrane helix bundle, *J. Biol. Chem. 276*, 38814−38819.
51. Simmerman, H. K., Kobayashi, Y. M., Autry, J. M., and Jones, L. R. (1996) A leucine zipper stabilizes the pentameric membrane domain of phospholamban and forms a coiled-coil pore structure, *J. Biol. Chem. 271*, 5941−5946.
52. Ramjeesingh, M., Huan, L. J., Garami, E., and Bear, C. E. (1999) Novel method for evaluation of the oligomeric structure of membrane proteins, *Biochem. J. 342*, 119−123.
53. Therien, A. G., and Deber, C. M. (2002) Oligomerization of a peptide derived from the transmembrane region of the sodium pump gamma subunit: effect of the pathological mutation G41R, *J. Mol. Biol. 322*, 583−550.
54. Beevers, A. J., and Kukol, A. (2006) Secondary structure, orientation, and oligomerization of phospholemman, a cardiac transmembrane protein, *Protein Sci. 15*, 1127−1132.
55. Bales, B. L. (2001) A definition of the degree of ionization of a micelle based on its aggregation number, *J. Phys. Chem. B 105*, 6798−6804.
56. Franzin, C. M., Gong, X. M., Thai, K., Yu, J., and Marassi, F. M. (2007) NMR of membrane proteins in micelles and bilayers: The FXYD family proteins, *Methods 41*, 398−408.
57. Tanford, C., and Reynolds, J. A. (1976) Characterization of membrane proteins in detergent solutions, *Biochim. Biophys. Acta 457*, 133−170.
58. Beguin, P., Crambert, G., Guennoun, S., Garty, H., Horisberger, J. D., and Geering, K. (2001) CHIF, a member of the FXYD protein family, is a regulator of Na,K-ATPase distinct from the gamma-subunit, *EMBO J. 20*, 3993−4002.
59. Meij, I. C., Koenderink, J. B., van Bokhoven, H., Assink, K. F., Groenestege, W. T., de Pont, J. J., Bindels, R. J., Monnens, L. A., van den Heuvel, L. P., and Knoers, N. V. (2000) Dominant isolated renal magnesium loss is caused by misrouting of the Na(+),K(+)-ATPase gamma-subunit, *Nat. Genet. 26*, 265−266.
60. Zamoon, J., Mascioni, A., Thomas, D. D., and Veglia, G. (2003) NMR solution structure and topological orientation of monomeric phospholamban in dodecylphosphocholine micelles, *Biophys. J. 85*, 2589−2598.
61. Metcalfe, E. E., Traaseth, N. J., and Veglia, G. (2005) Serine 16 phosphorylation induces an order-to-disorder transition in monomeric phospholamban, *Biochemistry 44*, 4386−4396.
62. Newton, A. C. (2003) Regulation of the ABC kinases by phosphorylation: protein kinase C as a paradigm, *Biochem. J. 370*, 361−371.
63. Vinton, B. B., Wertz, S. L., Jacob, J., Steere, J., Grisham, C. M., Cafiso, D. S., and Sando, J. J. (1998) Influence of lipid on the structure and phosphorylation of protein kinase C alpha substrate peptides, *Biochem. J. 330*, 1433−1442.
64. Sweadner, K. J., and Donnet, C. (2001) Structural similarities of Na,K-ATPase and SERCA, the Ca(2+)-ATPase of the sarcoplasmic reticulum, *Biochem. J. 356*, 685−704.

BI700391B